X-641-69-426

PREPRINT

NASA TM X- 63701

ENERGY DEPENDENCE OF HORIZONTALLY INCIDENT ATMOSPHERIC MUONS

KAICHI MAEDA

SEPTEMBER 1969

GSFC

GODDARD SPACE FLIGHT CENTER

GREENBELT, MARYLAND

X-641-69-426

ENERGY DEPENDENCE OF HORIZONTALLY INCIDENT ATMOSPHERIC MUONS

Kaichi Maeda

September 1969

Presented at the Eleventh International Conference on Cosmic Rays,
Budapest, Hungary, 1969

GODDARD SPACE FLIGHT CENTER
Greenbelt, Maryland

ENERGY DEPENDENCE OF HORIZONTALLY INCIDENT ATMOSPHERIC MUONS

Kaichi Maeda

ABSTRACT

Horizontally incident atmospheric muons and their parent particles travel one of the longest paths in the earth's atmosphere, leading to the largest possible atmospheric effects on the muon production process. Diffusion equations for cosmic ray mesons in the atmosphere are inadequate to treat these effects at large zenithal direction. The calculation is, therefore, made by modifying the Chapman function for the non-isothermal atmosphere, and computations are also applied to a mountain altitude, specifically for the laboratory at Mt. Chacaltaya (5200 m).

CONTENTS

ENERGY DEPENDENCE OF HORIZONTALLY INCIDENT ATMOSPHERIC MUONS

1. INTRODUCTION

The purposes of this paper are: first, to extend the author's previous calculation (Maeda 1964)* to higher energy and larger zenith angles; and second, to apply these extended calculations to the determination of the effects of atmospheric structure on the zenith angle distribution of the atmospheric muons. In particular, the direction of the maximum muon intensity as a function of muon energies at two different altitudes will be discussed. The atmospheric muon is defined by Wolfendale (1968).

2. COSMIC RAYS IN THE ATMOSPHERE

In M-1, variations of cosmic ray intensity in the atmosphere are expressed in integral form as a function of the atmospheric depth, x in g/cm^2, instead of the solutions of the so-called diffusion equations of cosmic rays in the atmosphere. In this expression, the following three features—which the diffusion equation cannot describe properly—are taken into account rigorously: (i) variation of air density with altitude, corresponding to changes in the vertical thermal structure of the atmosphere, (ii) variation of zenith angle along the straight oblique path with respect to the local horizontal due to the curvature of the earth's surface (see Figure 1), and (iii) a non-linear energy-range relation in the high energy regions due to the radiation loss and the direct pair-production loss, which dominate at extremely high energies. As was shown in M-1, these integrals agree with several approximate solutions of the so-called diffusion equations. In other words, the solution of these different equations corresponds to some special cases of the present results under several approximations. Notations and definitions in this paper are mostly the same as those used in M-1.

2.1 Differential Intensity of Cosmic Ray Mesons

The intensity of cosmic ray mesons, $n_i(E_i, x, \theta^*)$ with energy between E_i and $E_i + dE_i$ at the depth x with zenith angle between θ^* and $\theta^* + d\theta^*$ is given

*This will be referred to as M-1, later in this report.

by

$$n_i\left(E_i,\ x,\ \theta^*\right) = \int_0^x \frac{F\left(E_i'\right)}{L_c}\ e^{-D\left(E_i,\ x',\ \theta'\right)}\ \sec\theta^*\left(x'\right)\,dx' \qquad (2.1)$$

where

$$D\left(E_i,\ x',\ \theta^*\right) = \int_0^{x'} \frac{\sec\theta^*\left(x''\right)}{L_c}\,dx'' + \int_{x'}^{x}\left(\frac{1}{L_i} + \frac{B_i}{E_i''\left(x''\right)\rho\left(x''\right)}\right)\sec\theta^*\left(x''\right)dx'' .$$

The suffix i stands for pion (π) and kaon (k), respectively, and $F\left(E_i'\right)$ is the differential production spectrum of cosmic-ray mesons. The energy E_i'' at the depth x'' (at the production level) is related to E_i at the depth x by a range-energy relation.

2.2 Energy-Relation Between Muons and Parent Mesons

As was shown in M-1, the differential energy spectrum $n_\mu\left(E_\mu,\ x,\ \theta^*\right)$ of muons at production is given by

$$n_\mu\left(E_\mu,\ x,\ \theta^*\right) = \int_{E_\mu}^{E_\mu r_i^{\,2}} \frac{B_i\ \sec\theta^*}{E_i\ x}\ P\left(E_\mu\right) n_i\left(E_i,\ x,\ \theta^*\right)\,dE_i \qquad (2.2)$$

where

$$P\left(E_\mu\right) = \frac{1}{\left(1 - r_i^{\,2}\right)E_i}\ , \qquad r_i = \frac{m_\mu}{m_i}\ . \qquad (2.3)$$

2.3 Differential Intensity of the Atmospheric Muons

The differential energy spectrum $i_\mu\left(E,\ x_0, \theta\right)$ of muons at the depth x_0, arriving from the direction with zenith angle θ, is different from that of the

production $n_\mu (E_\mu, x, \theta^*)$ at the depth x, but is connected by the so-called "survival probability," $W(E, x_0, x, \theta)$, in the following way:

$$i_\mu (E, x_0, \theta) = \int_0^{x_0} n_\mu (E_\mu, x, \theta^*) W(E, x_0, x, \theta) dx , \qquad (2.6)$$

where the local zenith angle $\theta^* (x)$ at the depth x along the straight path of the muon, arriving at the depth x_0 with the zenith angle θ, is related to θ, as can be seen from Figure 1, by

$$\sin\theta^* (x) = \frac{R_z}{R_z + h(x)} \sin\theta , \qquad R_z = R_E + z . \qquad (2.7)$$

The survival probability $W(E, x_0, x, \theta)$ is given by

$$W(E, x_0, x, \theta) = \exp\left[- \frac{m_\mu c^2}{c\tau_\mu} \int_x^{x_0} \frac{\sec\theta^* (x')}{E_\mu (E, x', \theta)} \frac{dx'}{\rho(x')} \right] . \qquad (2.8)$$

2.4 The Energy Loss in the Atmosphere

Detailed studies of energy loss processes of muons have been made by several cosmic ray workers up to around 1000 GeV (Barrett et al., 1952; Ashton, 1961; Ozaki, 1962; Hayman et al., 1963). These works are, however, based on the underground experiments and results are expressed with respect to the Standard Rock. Since the energy loss process of muons has been known as essentially the same as that of electrons but with larger mass, their results, which depend on Z/A and Z^2/A of the medium, can be reduced to those in air by using Table 1. In Table 1 the density ρ, atomic number Z, atomic weight A, Z/A and Z^2/A of air and of the Standard Rock are shown for comparison.

The change in a muon's energy along its penetration path in the atmosphere can be calculated by using the average range-energy relation in air, which is derived from the empirical formula for the energy loss rate of muons, i.e.,

$$- \frac{dE}{d\xi} = a_e + b_e E , \qquad (2.9)$$

where $d\xi = dx \sec\theta^*(x)$ is a path element of the muon in the atmosphere, and the constants a_e, b_e are 2.5×10^{-3} (GeV/g cm^{-2}) and 2.5×10^{-6} (g/cm^2)$^{-1}$, respectively (M-1).

3. HORIZONTALLY INCIDENT COSMIC RAYS

At the mountain laboratories, the cosmic rays arriving from below the horizontal direction can be observed.

To calculate the intensities of these cosmic rays, the expression described in the previous section is not suitable because of the $\sec\theta^*$ term, which diverges at $\theta = 90°$ as the altitude $h(x)$ approaches that of the observation point, z. The calculation is made, therefore, by using the Chapman function instead of $\sec\theta^*$. The Chapman function is defined by the constant scale height atmosphere, i.e., the isothermal atmosphere (Chapman, 1931). This is, however, easily extended for the standard atmosphere, in which the isothermal stratosphere is situated above the polytropic (constant lapse rate) troposphere. The atmospheric depth, x (in g cm^{-2}) in the standard atmosphere is shown in Figure 2 as a function of altitude, z (in km).

3.1 In the Isothermal Atmosphere

All expressions in the previous sections are expressed by the Chapman function, the integral of $ch(\theta, \lambda)$ with respect to the local zenith angle, λ, along a straight path of muons in the atmosphere as follows:

$$i_\mu(E, x_0\theta) = \int_0^\theta \frac{b_i f_i}{E_\mu(\lambda)} n_i(E_i'\lambda) R_t(\theta) \operatorname{cosec}^2\lambda \, d\lambda \qquad (3.1)$$

$$n_i(E_i'\lambda) = \frac{F(E_i')}{\ell_c'} \int_0^\lambda e^{-D(E_i', \theta, \lambda')} ch(\theta, \lambda) \, d\lambda' \qquad (3.2)$$

$$D(E_i'\theta, \lambda') = \left(\frac{1}{\ell_n'} \int_0^{\lambda'} + \frac{1}{\ell_i'} \int_{\lambda'}^{\lambda} \right) ch(\theta, \lambda'') \, d\lambda'' + \frac{b_i}{E_i'} [\cot\lambda'']_{\lambda'}^{\lambda}, \qquad (3.3)$$

where

$$\ell'_{n,i,c} = L_{n,i,c}/\rho_0 \tag{3.4}$$

$$ch(\theta, \lambda') = R_t(\theta)\,\mathrm{cosec}^2\lambda'\,\exp-\left(\frac{R_t(\theta)\,\mathrm{cosec}\,\lambda' - R_E}{H}\right) \tag{3.5}$$

$$E_i' = \gamma_i E_\mu\,, \qquad \gamma_i = \frac{m_i}{m_\mu} \tag{3.6}$$

and

$$E_\mu(\lambda) \cong E + \left(a_e + b_e E\right)\rho_0 \int_\lambda^\theta ch(\theta, \lambda')\,d\lambda'\,. \tag{3.7}$$

3.2 In the Standard Atmosphere

Because of the difference in the atmospheric depth-height relation between the upper and lower atmosphere, i.e., above and below $h = h_t$, all terms containing $ch(\theta, \lambda)$ in the expressions in Section 3.1 must be replaced by $ch(b, \lambda)$ for $\lambda \leq \lambda_t$, and $c\ell(a, \lambda)$ for $\theta \geq \lambda \geq \lambda_t$, respectively. Corresponding to Equation (3.2), therefore, we get

$$n_i\left(E_i', \lambda\right) = F\left(E_i'\right)\frac{1}{\ell_c^s}\int_0^{\lambda_t} e^{-D_s(E_i', \lambda')}\,ch(b, \lambda')\,d\lambda'$$

$$+ \frac{1}{\ell_c^t}\int_{\lambda_t}^{\lambda} e^{-D_t(E_i', \lambda')}\,c\ell(a, \lambda')\,d\lambda'\,, \tag{3.8}$$

$$D_s\left(E_i', \lambda'\right) = \frac{1}{\ell_n^s}\int_0^{\lambda'} ch(b, \lambda'')\, d\lambda'' + \frac{1}{\ell_i^s}\int_{\lambda'}^{\lambda} ch(b, \lambda'')\, d\lambda''$$

$$+ \frac{b_i}{E_i'}(\cot\lambda - \cot\lambda'), \qquad \lambda \leq \lambda_t \tag{3.9}$$

$$\ell_{n,i,c}^s = L_{n,i,c}/A_s, \tag{3.10}$$

$$D_t\left(E_i', \lambda'\right) = \frac{1}{\ell_n^t}\int_{\lambda_t}^{\lambda'} c\ell(a, \lambda'')\, d\lambda'' + \frac{1}{\ell_i^t}\int_{\lambda'}^{\lambda} c\ell(a, \lambda'')\, d\lambda''$$

$$+ \frac{b_i}{E_i}(\cot\lambda - \cot\lambda''), \qquad \theta \geq \lambda \geq \lambda_t \tag{3.11}$$

$$\ell_{n,i,c}^t = L_{n,i,c}/A_t. \tag{3.12}$$

Similarly, the relation between the muon's energy $E_\mu(\lambda)$ at the production level $h(x)$ and E at the observing altitude z with zenithal angle, θ is, instead of Equation (3.7), given by

$$E_\mu(\lambda) = E + \left(a_e + b_e E\right)\left[A_s\int_{\lambda}^{\lambda_t} ch(b, \lambda')\, d\lambda' + A_t\int_{\lambda_t}^{\theta} c\ell(a, \lambda')\, d\lambda'\right]. \tag{3.13}$$

It should be noted that $ch(b, \lambda)$ and $c\ell(a, \lambda)$ are defined only for $\lambda \leq \lambda_t$ and $\theta \geq \lambda \geq \lambda_t$, respectively, i.e.,

$$ch(b, \lambda) = 0 \qquad \text{for} \qquad \lambda \geq \lambda_t,$$

$$c\ell(a, \lambda) = 0 \qquad \text{for} \qquad \lambda \leq \lambda_t. \tag{3.14}$$

It should also be noted that most data from muon intensity measurements are integral spectra which are given by

$$I_\mu (E_0, x_0, \theta) = \int_{E_0}^{\infty} i_\mu (E, x_0, \theta) \cdot dE \qquad (3.15)$$

where E_0 is the cut-off energy defined by conditions of the muon-detector and $i_\mu (E, x_0, \theta)$ is given by (3.1).

4. NUMERICAL CALCULATIONS AND RESULTS

4.1 In the Isothermal Atmosphere

Directional differential intensities of the atmospheric muons, $i_\mu (E, x_0, \theta)$, which are calculated by using Equations (3.1) ~ (3.7), are shown in Figure 3(a) for $x_0 = 1030$ g/cm^2 ($z = 0$ km, sea level) and (b) for $x_0 = 530$ g/cm^2 ($z = 5.2$ km). In these figures, intensities are plotted (in GeV^{-1} cm^{-2} sec^{-1} ster^{-1}) against the zenith angle, θ, with energy E (in GeV) at the observing point as a parameter. In all cases, the attenuation mean free path L_n of the primary cosmic rays and the nuclear absorption mean free path of L_π pions are both assumed to be 120 g/cm^2. To see the difference between warm and cold atmospheric conditions, results are also shown for two temperatures, $T = 340°$ and $T = 170°$K as heavy and light curves, respectively. The warm and cold atmospheres correspond to scale heights of 10 km and 5 km, respectively.

As can be seen from these figures, the horizontally incident atmospheric muon intensity in the isothermal atmosphere decreases with the atmospheric temperature, both at sea level and at mountain altitudes. It should be noted, however, that in near-vertical directions, the high energy muon intensity increases with atmospheric temperature increase; this has been known as the "positive temperature effect" on the cosmic ray intensity (Duperier, 1951; Barrett et al., 1952).

On the other hand, at low energies (below around 100 GeV), the muon intensity in near-vertical directions decreases with increase of atmospheric temperature, and this is well known as the "negative temperature effect" on cosmic ray intensity (Blackett, 1938; Maeda and Wada, 1954; Dorman, 1957).

In Figure 4, the energy dependence of directional differential muon intensity, $i_\mu (E, x_0, \theta)$ is shown (a) for sea level and (b) for $z = 5.2$ km. Corresponding to Figures 3(a) and (b), two cases of the atmospheric temperature, 340°K and 170°K are shown by light and heavy lines, respectively, in Figures 4(a) and (b). Since the energy dependence of $i_\mu (E, x_0, \theta)$ is indicated in Figure 3, only two cases of the zenith angle are shown in Figure 4, i.e., (a) for sea level $\theta = 0°$, 85°, and 90°; and (b) for $z = 5.2$ km altitude, $\theta = 0°$, 90°, and 92.3°, respectively.

One conspicuous feature of $i_\mu (E, x_0, \theta)$ is the direction of the maximum muon intensity, which is not only a function of energy, E, but also of atmospheric depth (i.e., altitude) x_0, of temperature T, of the atmospheric structure, and of the mean free path L_i of the muons, parent particles. This is shown in Figure 5, where the zenith angle of the maximum muon intensity, $\theta_{max}(E)$, is plotted against the muon energy at the observation point, E (in GeV), for sea level and mountain altitudes (5.2 km). To see the dependence on the atmospheric temperature, two cases, T = 340°K (H = 10 km) and T = 170°K (H = 5 km), are presented. For a comparison, one case for the standard atmosphere is also shown in Figure 5. From this figure, one can see that: (i) The direction of the maximum muon intensity is almost independent of energy at very high energies (above around 10 TeV). (ii) At low energies (below around 100 GeV), the direction of the maximum approaches zenith rapidly with decreasing energy. (iii) The zenith angle of the maximum muon intensity is larger at mountain altitudes than at sea level for the same muon energy at the observing point. (iv) The zenith angle of maximum intensity is also larger in the cold atmosphere than in the warm atmosphere. (v) Obviously, the dependence of θ_{max} on the atmospheric structure is more sensitive in the lower energies than in the higher; and in the latter, θ_{max} approaches 90° almost independently of energy E.

4.2 In the Standard Atmosphere

Because of the existence of a vertical temperature gradient in the lower part of the actual earth's atmosphere, the rate of increase of atmospheric depth, x, with decreasing altitude, h, is less in the lower atmosphere (the troposphere) than in the upper atmosphere (the isothermal stratosphere), as is shown in Figure 2.

Since the decay rate of muons in flight is inversely proportional to their energy, which decreases with penetration depth in the atmosphere, the intensity of muons arriving deep in the atmosphere with a given initial energy differs from that calculated for the isothermal atmosphere, especially in the near-horizontal directions.

Corresponding to Figure 3, the directional integral intensity of atmospheric muons produced by pions $I_\mu (E_0, x_0, \theta)$ is shown in Figure 6(a) for sea level and

(b) for a mountain altitude, $z = 5.2$ km. Similarly, in Figure 7, $I_\mu (E_0, x_0, \theta)$ corresponding to kaon-produced muons is shown (a) for sea level and (b) for a mountain altitude, $z = 5.2$ km.

Figure 8 shows the energy dependence of the zenith angle of the maximum muon intensity, $\theta_{max}(E)$ at (a) sea level and (b) a mountain altitude $z = 5.2$ km. To see the difference in θ_{max} due to different values of the nuclear absorption mean free path of muon-producing mesons, three cases are indicated, assuming L_i to be equal to $1/2\ L_n$, L_n and $2L_n$ where L_i is the attenuation mean free path of pion-producing cosmic-ray primaries, i.e., $i = \pi$ for pions and $i = k$ for kaons. Figure 8 indicates that the smaller L_i, the larger $\theta_{max}(E)$ for the same energy E. In other words, the zenith angle dependence of atmospheric muons of a given energy produced by hypothetical mesons with a small absorption mean free path (i.e., a larger cross section for the nuclear absorption) is the same as that of the muons produced by the same mesons with a larger mean free path (i.e., small cross section for nuclear absorption in air) at higher energy. Since these zenith angle dependences of the atmospheric muons are due to the competition process between the nuclear absorption of muon-producing mesons, which is proportional to $1/L_i$, and the decay in flight of these mesons in the upper atmosphere, which is proportional to B_i/Ex, the result for small L_i can be reproduced approximately by large L_i with larger energy, as is discussed in M-1. The decay factor of the kaon is larger than that of the pion. Thus, to produce the same zenith angle dependence of muon intensity, the energy of the kaon must be roughly seven times larger than that of the pion. This is also shown in Figure 8 assuming $L_k = 1/2\ L_n$, $L_k = L_n$, and $L_k = 2L_n$.

5. DISCUSSION

An important matter related to the present calculation is the so-called "$\sec\theta$-law" for the zenithal distribution of cosmic-ray muons (Bergeson et al., 1967; 1968). As can be seen from Figures 3-6 this is only approximately correct for small zenith angles.

The difference in the zenith angle distribution of high energy muons between sea level and mountain altitudes ($z = 5.2$ km) shown in Figures 3-6, can be summarized as follows: (i) Below around 500 GeV, the zenithal distribution, particularly the direction of the maximum muon intensity, changes with the absorption mean free path of the muons' parent particles as well as with the abundance of kaons vs pions. (ii) Above 1 TeV, the zenith angle dependence and the direction of the maximum muon intensity are almost independent of the characteristics of parent particles and rather dependent on the atmospheric structure.

Further details of the present calculations on the atmospheric muons will be discussed elsewhere (Maeda, 1970).

REFERENCES

Ashton, F., Proc. Phys. Soc. 77, 587 (1961).

Barrett, P. H., L. M. Bollinger, G. Cocconi, Y. Eisenberg and K. Gresen, Rev. Mod. Phys. 24, 133 (1952).

Bergeson, H. E., J. W. Keuffel, M. O. Larson, E. R. Martin and G. W. Mason, Phys. Rev. Letters 19, 1487 (1967).

Bergeson, H. E., J. W. Keuffel, M. O. Larson, G. W. Mason and J. L. Osborne, Phys. Rev. Letters 21, 1089 (1968).

Blackett, P. M. S., Phys. Rev. 54, 973 (1938).

Chapman, S., Proc. Phys. Soc. 43, 483 (1931).

Dorman, L. I., Cosmic Ray Variations (Eng. transl.) (1957).

Duperier, A., Nature 167, 312 (1951).

Hayman, P. J., N. S. Palmer and A. W. Wolfendale, Proc. Phys. Soc. 80, 800 (1962).

Maeda, K., J. Geophys. Res. 69, 1725 (1964).

Maeda, K., To be submitted to J. Atmos. Terr. Phys. (1970).

Maeda, K. and M. Wada, J. Sci. Res. Inst., Tokyo 48, 71 (1954).

Ozaki, S., J. Phys. Soc., Japan 17, 330 (1962).

Wolfendale, A. W., Nature 219, 1215 (1968).

Table 1

Physical Constants of the Air and the Standard Rock

Average Value	The Air	The Standard Rock
ρ, density	1.25×10^{-3} (g/cm^3)	2.65 (g/cm^3)
Z, atomic number	7.37**	11.
A, atomic weight	14.78**	22.
Z/A*	0.499	0.5
Z^2/A*	3.675	5.5

*The average values of Z/A and Z^2/A are calculated by $\Sigma_i f_i Z_i/A_i$ and $\Sigma_i f_i Z_i^2/A_i$, respectively, where f_i is fractional weight.

**Rossi (1952), p. 295.

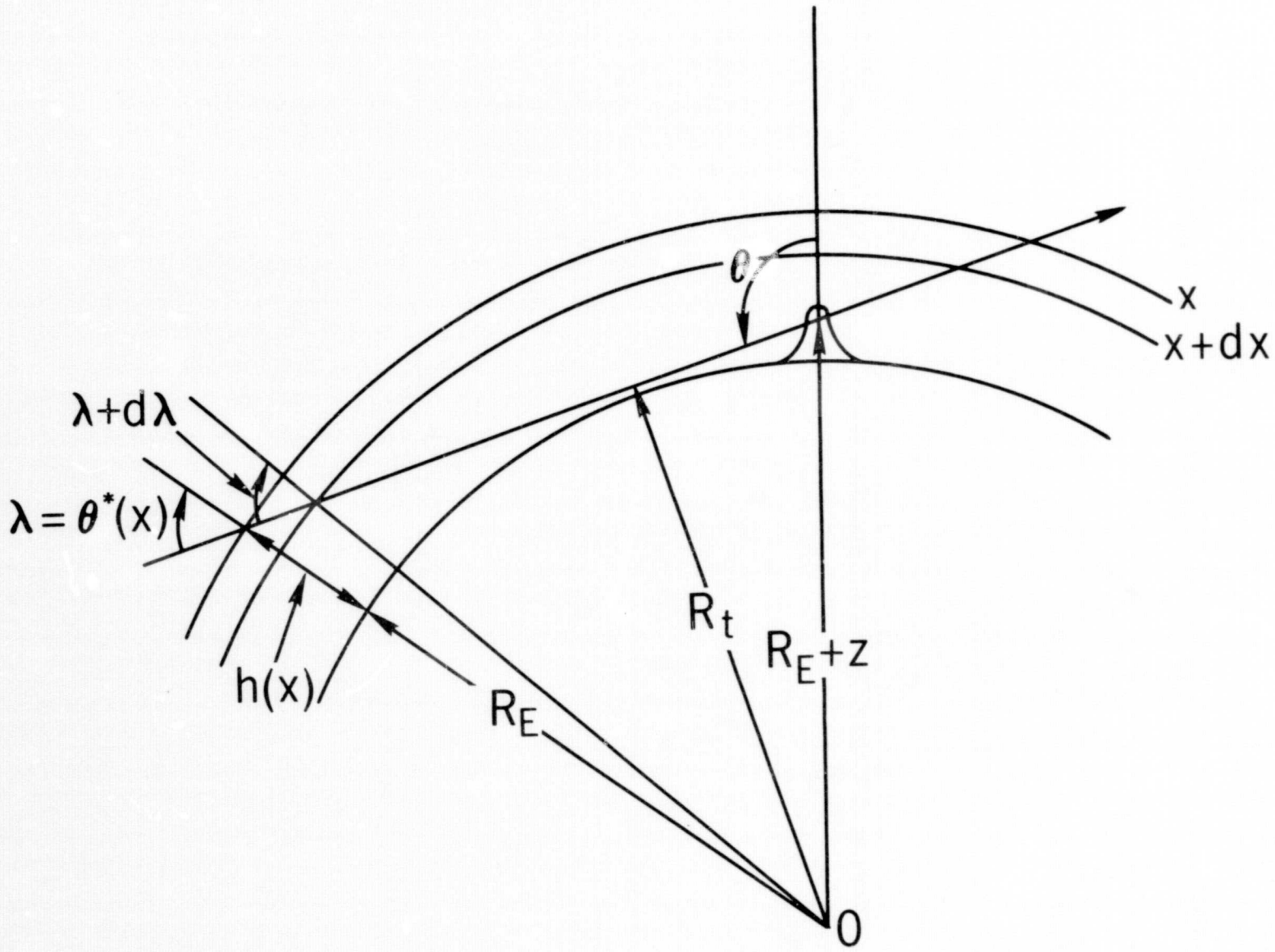

Figure 1. Geometric relation between the zenith angle θ at the atmospheric depth x_0 and the local zenith angle $\lambda = \theta^*(x)$ at the depth x in the atmosphere. R_E is the earth's radius and h(x) is the height of the level of atmospheric depth x.

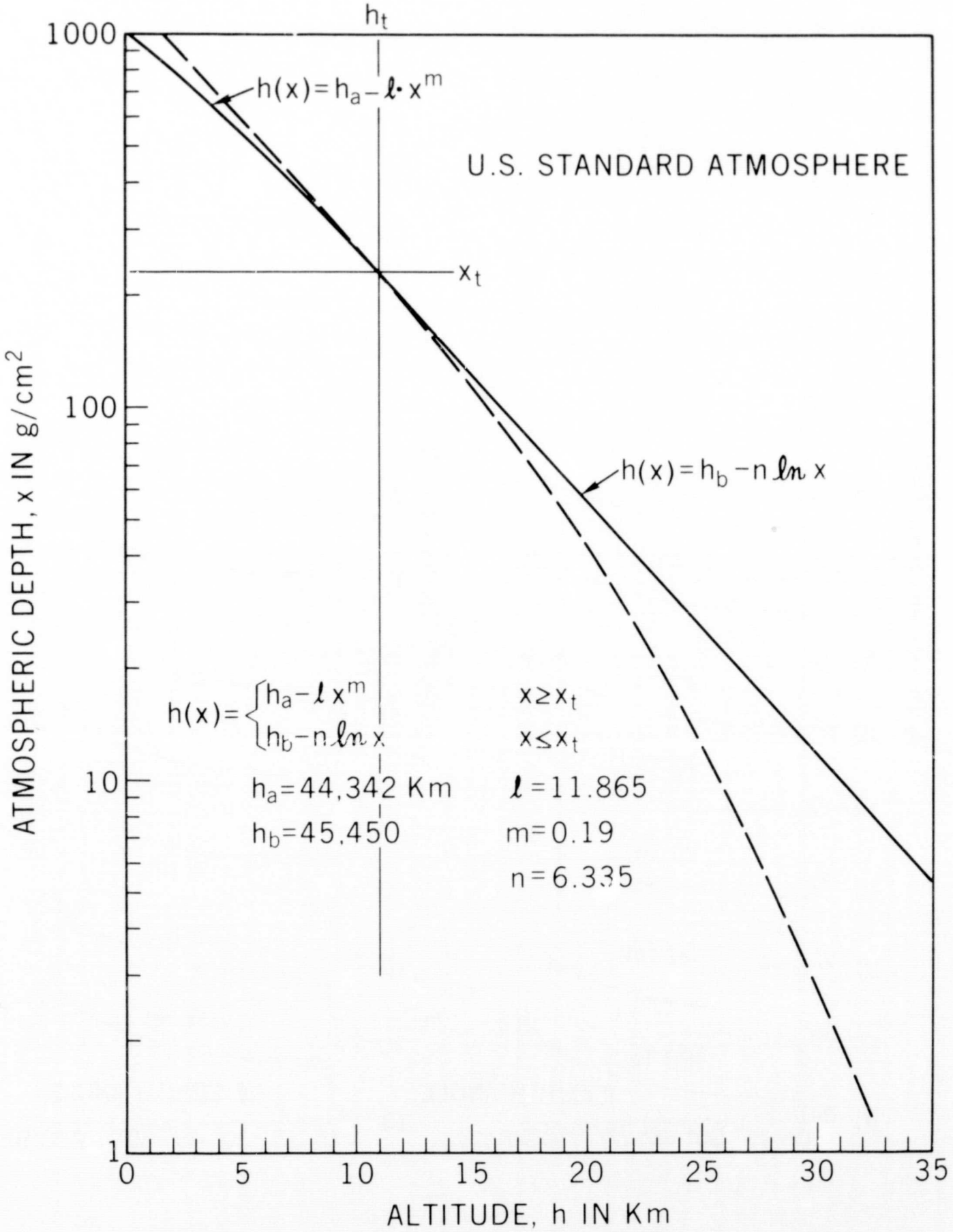

Figure 2. Comparison of the atmospheric depth-altitude relation in the standard atmosphere and empirical formula. Dashed lines correspond to the extrapolations of the formula beyond applicable altitude range.

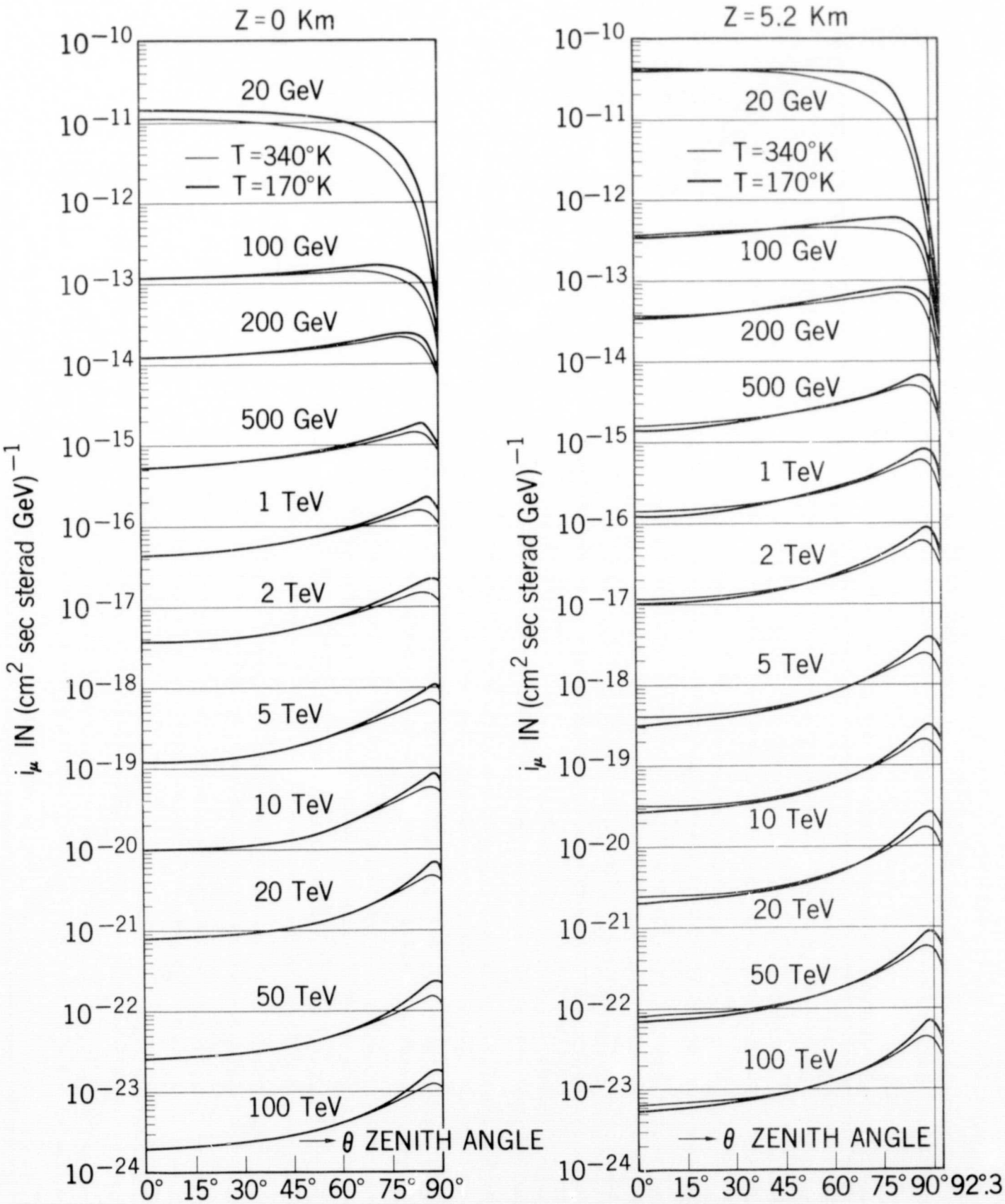

Figure 3. Zenith angle dependence of the differential intensity of atmospheric muons in the isothermal atmosphere, $i_\mu(E, x_0, \theta)$ in cm^{-2} sec^{-1} $ster^{-1}$ GeV^{-1}, plotted against zenith angle θ, with the energy of muons at the observation point, E (in GeV), as a parameter. (a) for sea level, $x_0 = 1030$ g/cm^2 (z = 0 km) and (b) for mountain altitudes $x_0 = 530$ g/cm (z = 5.2 km). Heavy and light curves correspond to the intensity in the warm (T = 340°K, H = 10 km) and cold atmosphere (T = 170°K, H = 5 km), respectively.

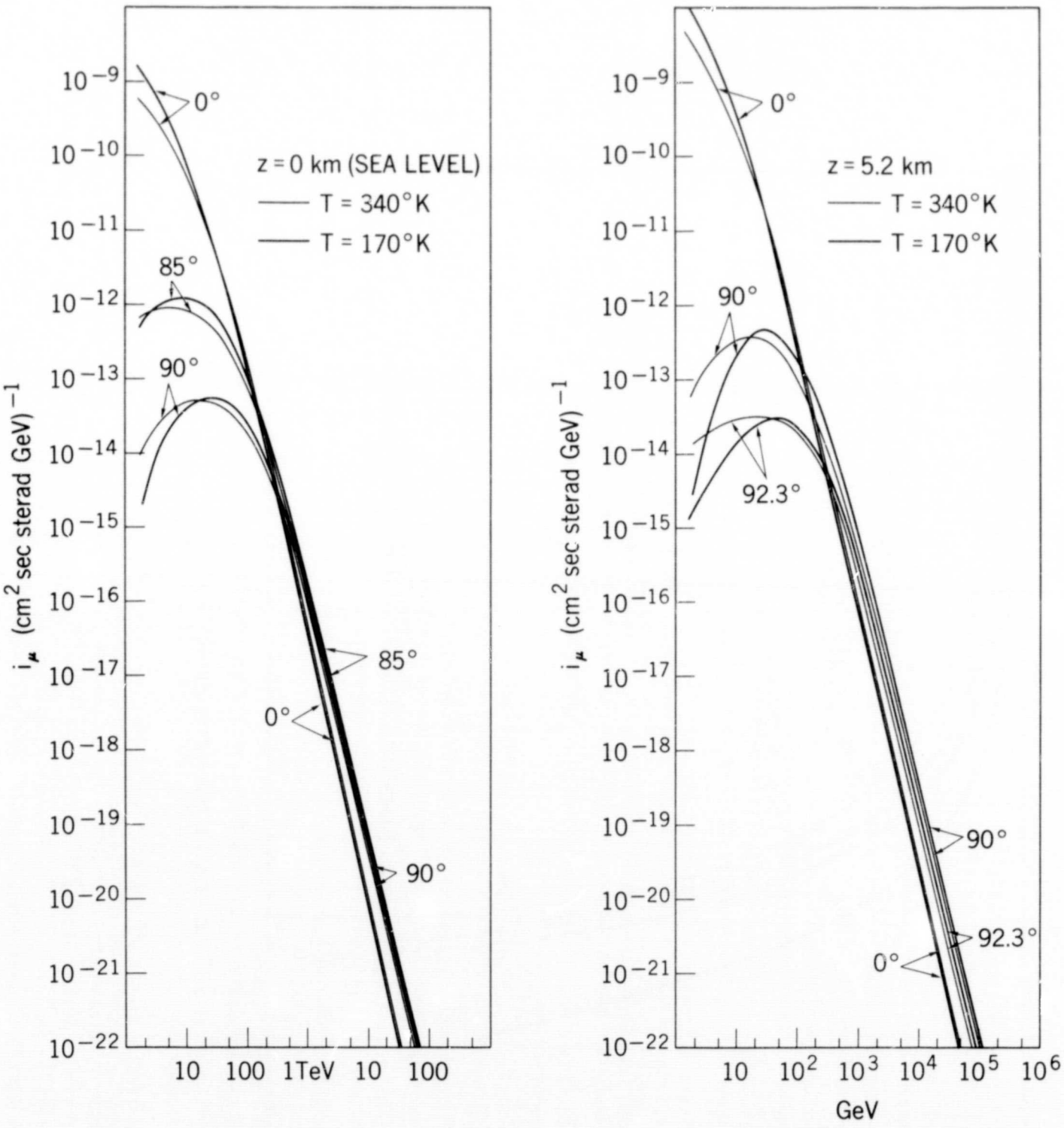

Figure 4. Energy dependence of the directional intensity of atmospheric muons in the isothermal atmosphere, $i_\mu(E, x_0, \theta)$ in cm^{-2} sec^{-1} $ster^{-1}$ GeV^{-1}, plotted against energy in GeV at the observation point: (a) for sea level (z = 0 km), $\theta = 0°$, 85°, and 90°; and (b) for mountain altitudes (z = 5.2 km), $\theta = 0°$, 90°, and 92.3°. Light and heavy curves correspond to intensities in the warm (T = 340°K) and the cold atmosphere (T = 170°K) respectively.

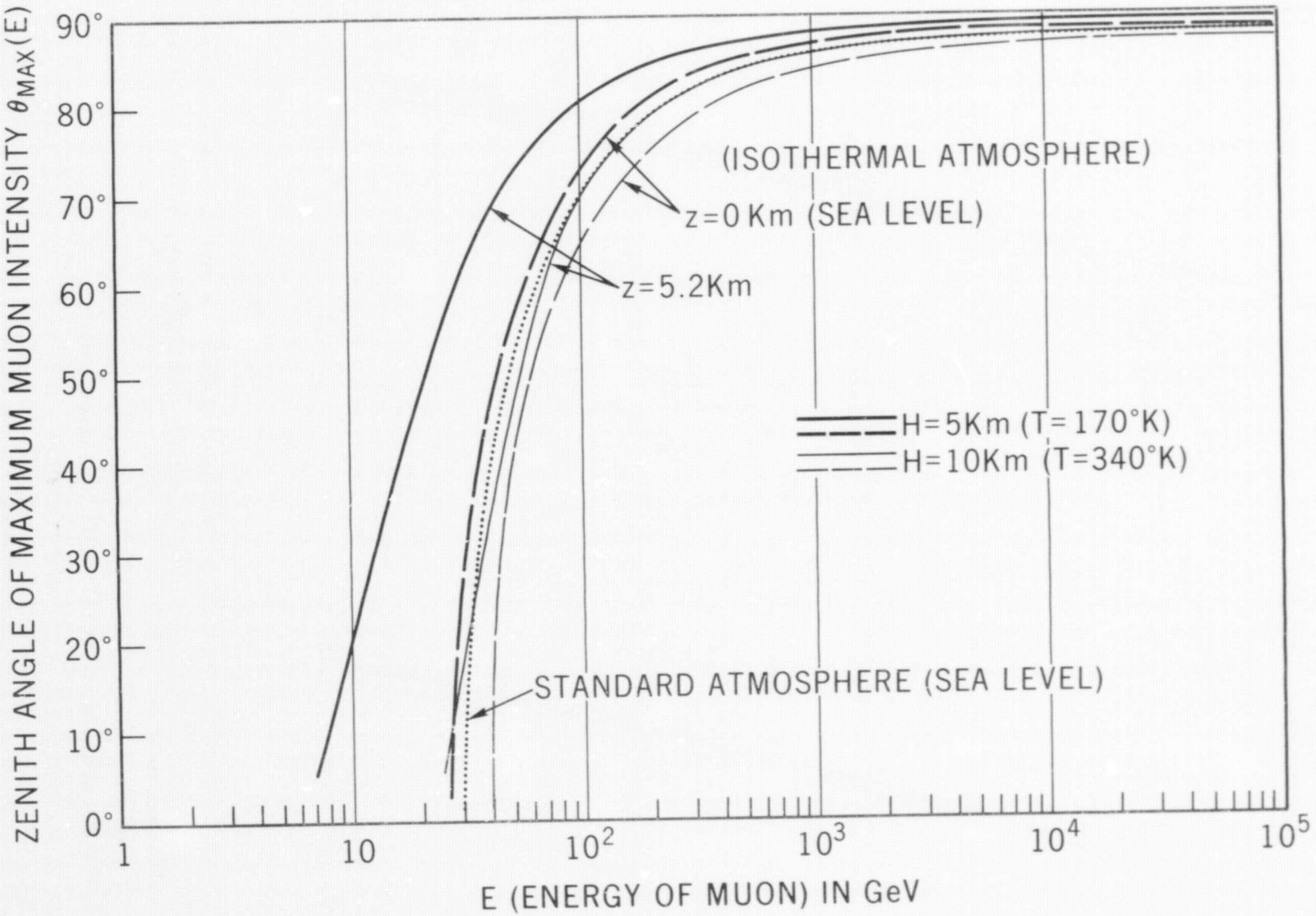

Figure 5. The energy dependence of the zenith angle of maximum atmospheric muon intensity θ_{max} (E), in the isothermal atmosphere, plotted against muon energy E in GeV. Curves are shown for sea level (x_0 = 1030 g/cm^2) and for mountain altitudes (x_0 = 530 g/cm^2) by dashed and solid lines, respectively. For each curve, two cases of atmospheric temperature are indicated by light curves for intensities in the warm atmosphere (T = 340°K), and by heavy curves for those in the cold atmosphere (T = 170°K). A dotted line corresponds to the results in the Standard Atmosphere, which is shown for a comparison, especially at lower energy (below 100 GeV).

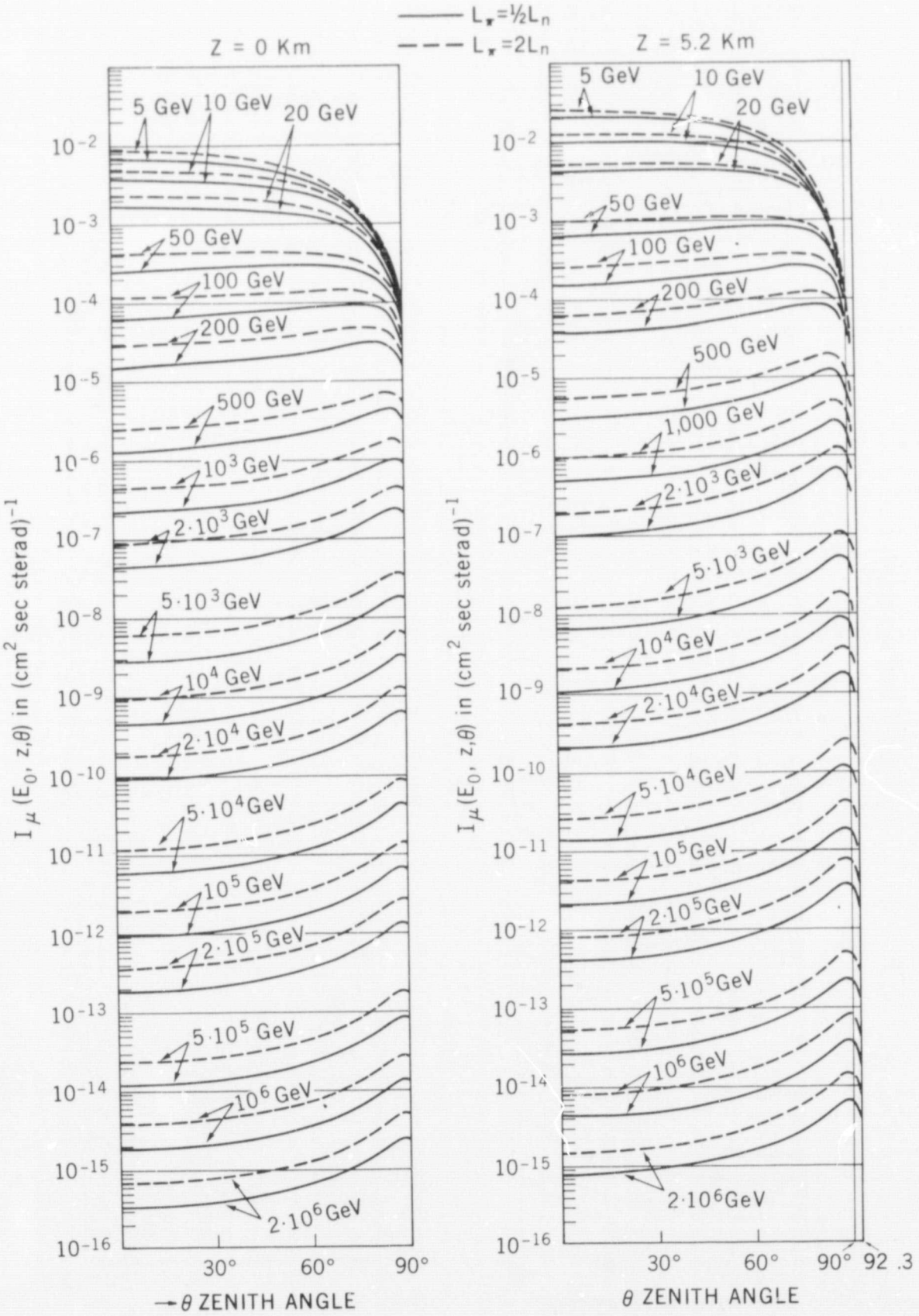

Figure 6. Zenith angle dependence of the directional intensity of atmospheric muons (integral spectra) produced by the decay of pions in the Standard Atmosphere $I_\mu(E_0, x_0, \theta)$ in $cm^{-2}\ sec^{-1}\ ster^{-1}$ plotted against the zenith angle: (a) for sea level ($x_0 = 1030\ g/cm^2$) and (b) for mountain altitudes ($z = 5.2$ km, $x_0 = 530\ g/cm^2$). Full lines and dashed lines correspond to $L_\pi = L_n/2$ and $L_\pi = 2L_n$, respectively ($L_n = 120\ g/cm^2$). The cut-off energy of the spectrum is E_0.

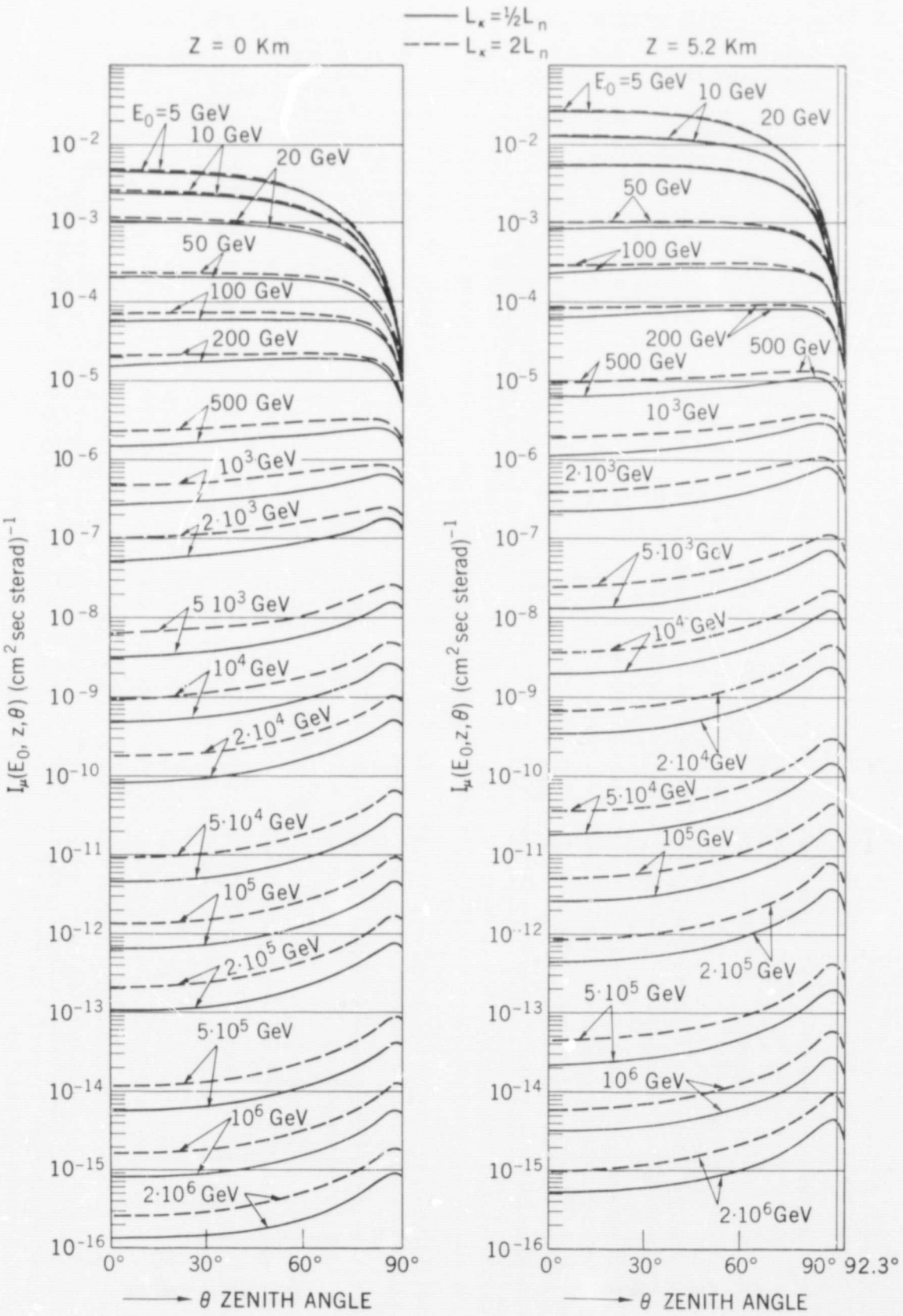

Figure 7. The same as Figure 6 except for atmospheric muons produced by the decay of kaons. (a) and (b) represent sea level and mountain altitudes (z = 5.2 km). Solid and dashed curves correspond to $L_k = L_n/2$, and $L_k = 2L_n$, respectively (L_n = 120 g/cm^2).

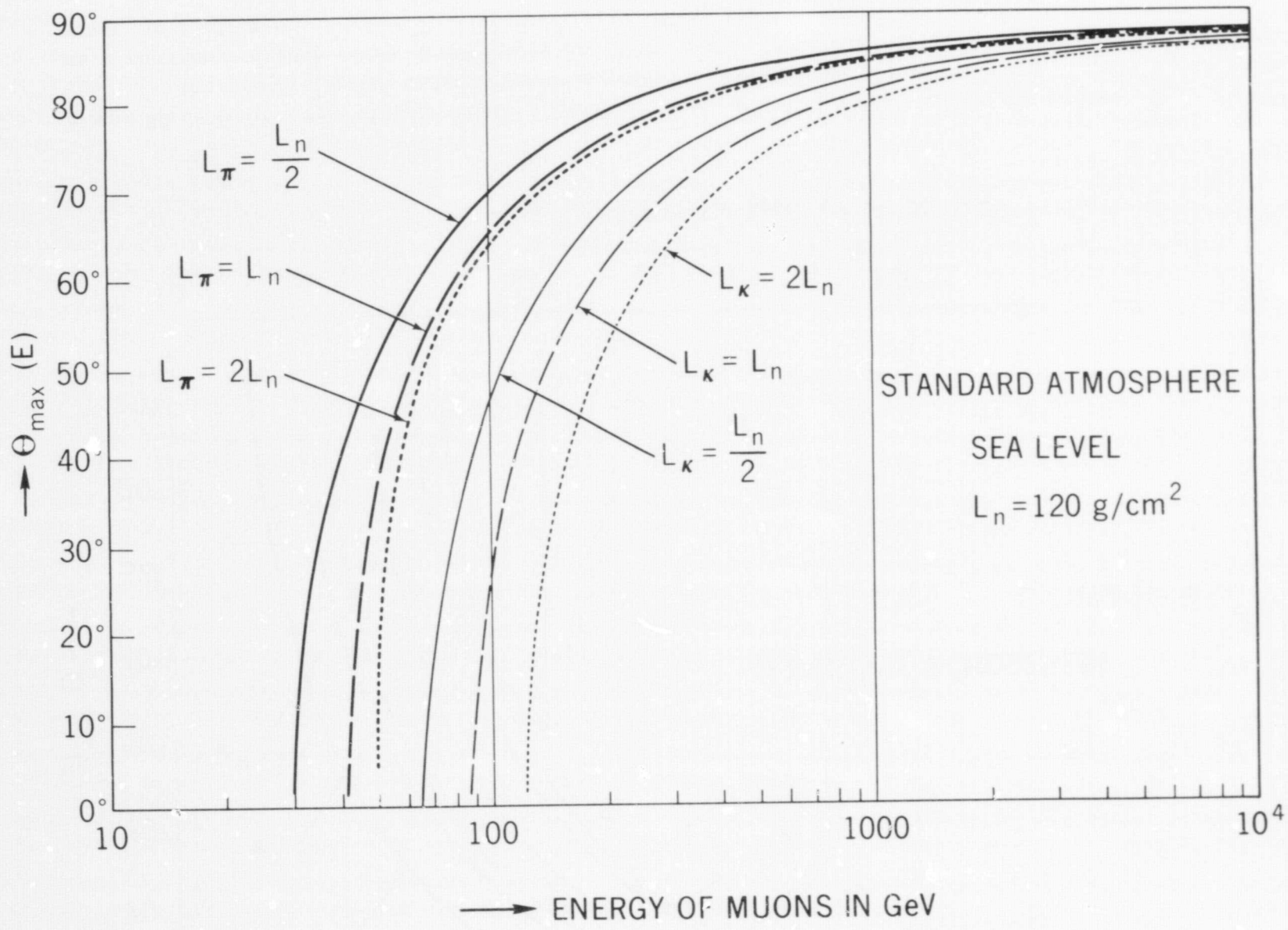

Figure 8(a). Zenith angle of the maximum atmospheric muon intensity in the standard atmosphere, θ_{max}, plotted against to the energy of muons at the observation point for sea level ($z = 0$). L_π and L_k are taken as a parameter of each curve, where heavy and light curves represent the pion-produced and kaon-produced muons, respectively.

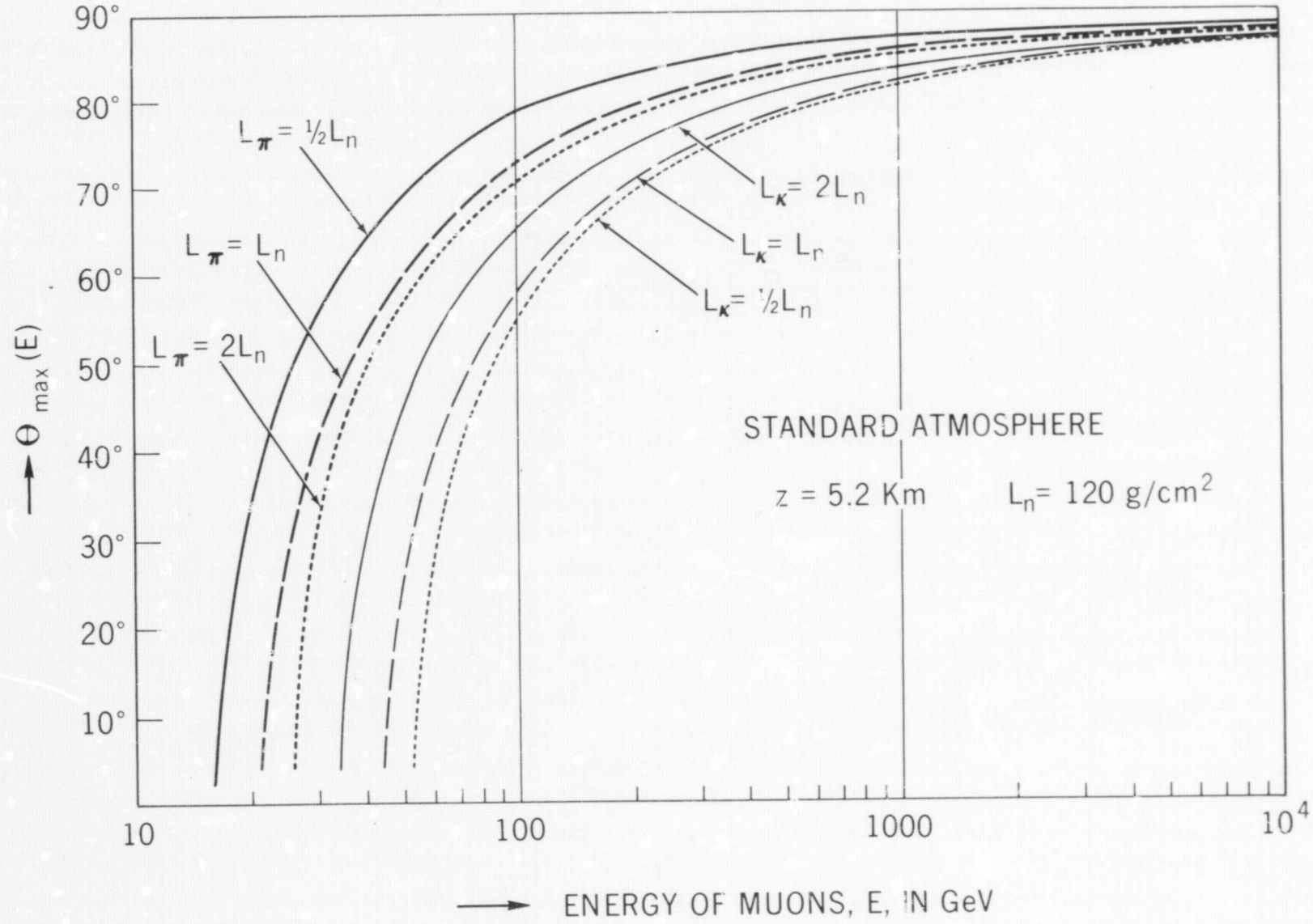

Figure 8(b). Zenith angle of the maximum atmospheric muon intensity in the standard atmosphere, θ_{max}, plotted against to the energy of muons at the observation point for mountain altitudes (z = 5.2 km). L_π and L_k are taken as a parameter of each curve, where heavy and light curves represent the pion-produced and kaon-produced muons, respectively.